Microscopic Susceptibility Variation and Transverse Relaxation for the De Facto Brain Tumor Microvasculature

D. Bonekamp[1], E. Kim[2], B. D. Ward[3], J. Zhang[1], and A. P. Pathak[1]

[1]Department of Radiology and Radiological Science, Johns Hopkins University, Baltimore, MD, United States, [2]Department of Biomedical Engineering, Johns Hopkins University, Baltimore, MD, United States, [3]Department of Biophysics, Medical College of Wisconsin, Milwaukee, WI, United States

INTRODUCTION: Despite knowledge of the molecular basis of angiogenesis in brain tumors and the development of imaging biomarkers of angiogenesis (e.g. susceptibility-based blood volume and vessel size index), the relationship between them remains poorly understood. Elucidation of this relationship requires biophysical models that incorporate accurate representations of the brain tumor vasculature [1, 2]. The difficulties in obtaining such data from patients, in conjunction with development of mouse tumor models have made the murine brain an indispensable tool for resolving such issues [3]. Here for the first time, we investigate the relationship between brain tumor angiogenesis and susceptibility-based contrast MRI by incorporating the "real" or *de facto* brain vasculature in a state-of-the-art computational model of MR image contrast called the *finite perturber method* (FPM) [1]. The specialty of the FPM is that it enables us to study susceptibility-induced contrast arising from *arbitrary* microvascular geometries in 3D, such as those typically observed during tumor angiogenesis. In previous work, we employed the FPM to demonstrate that the susceptibility-based MRI signal depends on the angiogenic stage of the tumor [4]. However, in that study, the microvascular architecture was generated *in silico*. In this study, we employed magnetic resonance microscopy (μMRI) to obtain the microvasculature of an entire 9L gliosarcoma xenograft-bearing mouse brain. Incorporating these 3D data into the FPM enabled comparison of the effect of both, the normal brain vasculature and brain tumor vasculature on the observed susceptibility-based MR contrast.

METHODS: The digitized, 3D microvasculature of an entire 9L tumor-bearing murine brain was acquired using μMRI according to the protocol described in [3]. Using the *finite perturber model* (FPM) we conducted a series of simulations to compare the effect of tumor and normal mouse brain microvasculature on the gradient-echo (GE) and spin-echo (SE) MRI signals. In the FPM approach, the underlying vessel geometry is divided into minute "perturbers". To calculate the field shift at a given point, the shift due to each perturber is calculated independently, and the total field shift calculated as the sum of the shifts from every perturber. The field shift arising from the entire vascular structure is computed in the Fourier domain as described in [1]. The MRI signal was simulated for the digitized, 3D representation of the entire mouse brain vasculature containing the 9L tumor xenograft. The 3D R2* and R2 maps were computed for the whole brain using the following biophysical parameters: B_0=1.5T, $\Delta\chi$=1×10-7 (~3.6mM Gd-DTPA), GETE=60ms, SETE=60ms, dt=0.1ms, unrestricted diffusion coefficient=1.0 μm^2/ms, with 10000 protons randomly placed in the simulation universe. 3D ROI–based analysis was carried out. The tumor xenograft ROI fractional volume (FV) was ~15%, and contralateral brain ROI FV was ~4%.

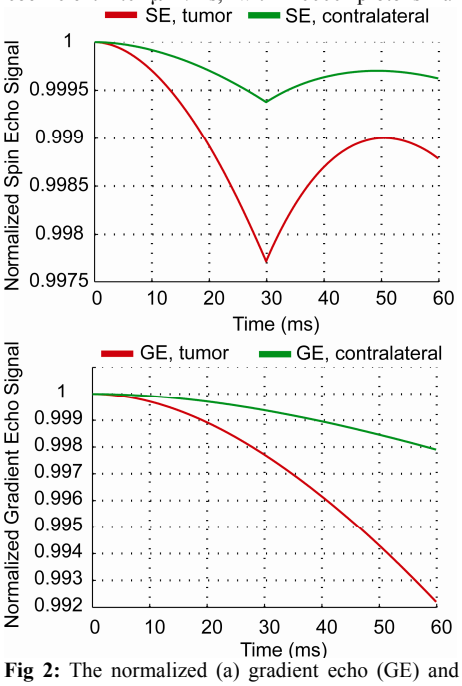

Fig 2: The normalized (a) gradient echo (GE) and (b) spin echo (SE) signals differ substantially between normal brain and tumor ROI.

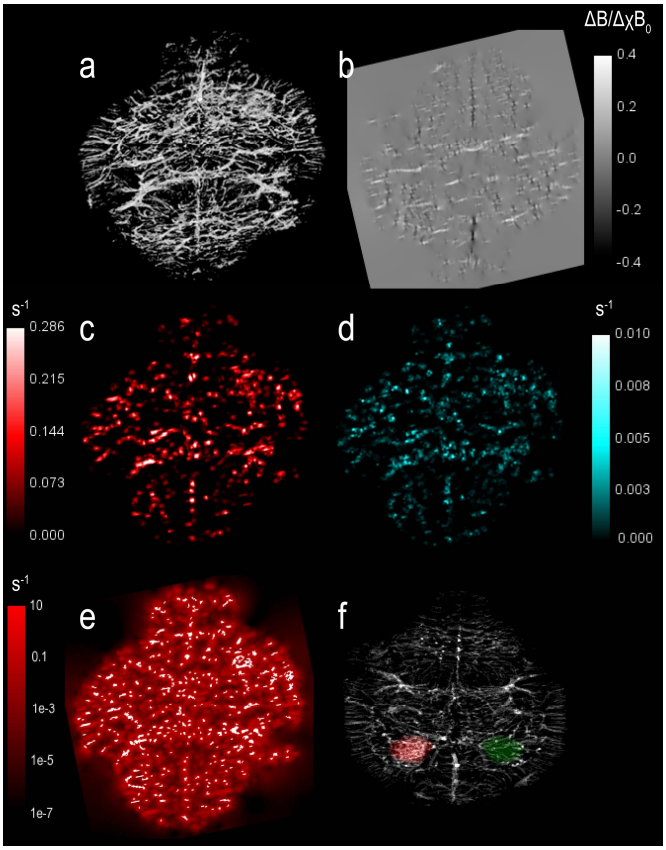

Fig 1: (a) 3D rendering of the digitized murine vasculature. (b) Axial slice through the 3D field map generated from the "real" vasculature in (a). Slices through (c) the 3D $\Delta R2^*$ and (d) $\Delta R2$ maps. (e) Overlay of the $\Delta R2^*$ map (red) after logarithmic transform and the vascular map (white). (f) In a different mouse brain, tumor ROI (red) and contralateral ROI (green) are overlaid on an axial projection through the murine brain microvasculature.

RESULTS: **Fig. 1a** illustrates the high-resolution (~40μm) coverage of the whole brain vasculature achievable with μMRI. **Fig. 1b-d** demonstrates the derivation of high-resolution magnetic field perturbation, ΔR2 and ΔR2* maps, respectively from which spatially selective ROI analysis of the MR signal was performed. **Fig. 2** illustrates the effect of the contralateral brain and tumor microvasculature on the evolution of the GE and SE signals, respectively. One can clearly see that the MR signal in both cases is profoundly affected by the presence of abnormal tumor microvessels.

DISCUSSION: The data presented in **Fig. 2** indicate that MR signals derived from the *de facto* mouse brain vasculature for a typical susceptibility-based imaging protocol differ substantially between normal brain and tumor ROIs. This effect is more pronounced for the GE signal, which is consistent with data from Boxerman et al. in which Monte Carlo simulations demonstrated the sensitivity of the GE signal to vessels of all sizes [5]. For the first time, the effect of the entire vascular network of a mouse brain can be studied with this approach. We are currently in the process of correlating *in-vivo* MRI data directly with the predictions of the FPM. Additionally, we are currently working on quantifying the dependence of the relaxation rate ratio (ΔR2*/ΔR2) on the underlying vessel size distribution, contrast agent dose and magnetic field strength.

CONCLUSIONS: In order to develop accurate biomarkers of angiogenesis and anti-angiogenic therapies in brain tumors, one needs to develop a quantitative understanding of the relationship between pathological vascular changes and corresponding imaging biomarkers (e.g. susceptibility-based blood volume and vessel size index). The novel integration of the *de facto* tumor vasculature into mathematical models such as the FPM is a promising first step towards this goal.

REFERERENCES: **1.** Pathak et al, *NeuroImage*, 2008. **2.** Kiselev *MRM*, 46(6):2001. **3.** Pathak et al., ISMRM, 284, 2008. **4.** Pathak et al., ISMRM, 3832, 2008. **5.** Boxerman et al., *MRM*, 34(4):1995.

ACKNOWLEDGEMENTS: Research supported by RSNA Toshiba Medical Systems Seed Grant. Nicole Benoit for technical assistance with the animals.